

GT2011-4538

FLAME TRANSFER FUNCTION MEASUREMENTS IN A SINGLE NOZZLE COMBUSTOR

Shawn D. Wehe
 GE - Global Research
 Niskayuna, NY, USA

Hejie Li
 GE - Aviation
 Cincinnati, OH, USA

Keith R. McManus
 GE - Global Research
 Niskayuna, NY, USA

ABSTRACT

This paper describes an experimental investigation of Flame Transfer Function (FTF) behavior where the response of a swirl-stabilized, natural gas fueled combustor is measured for partially premixed conditions. Controlled perturbations of the combustor inlet flows are produced using a siren and the combustor response is observed using several measurement techniques. The fuel/air equivalence ratio fluctuation is measured using a diode laser absorption sensor operating near 1.6 μm . Measurements of global heat release perturbations are obtained using a three-color optical emission technique and velocity measurements are obtained using the two-microphone method. FTFs are derived from these measurements for a frequency range commensurate with field-observed tones. Typical experimental investigations of dynamic signals involve the use of Fourier methods to obtain average signal amplitudes and phase. In this investigation, standard Fourier techniques are used to verify the driving frequencies, but they are coupled with a homodyne detection algorithm to measure time-dependent gain and phase behavior of a FTF.

NOMENCLATURE

C_N	Power-law coefficient matrix
f	Frequency
FTF	Flame Transfer Function
H_{fuel}	Fuel chemical enthalpy
i	Species
I_i	Chemiluminescence intensity
\bar{I}	Average chemiluminescence intensity
j	$\sqrt{-1}$
k_i	Chemiluminescence intensity coefficient
L	Characteristic burner dimension
m_{Air}	Air mass flow rate

m_{Fuel}	Fuel mass flow rate
N	Number of measured chemiluminescent species
p	Pressure
q'	Heat release perturbation
\bar{q}	Average heat release rate
Q	Heat release rate
t	Time
v'	Velocity perturbation
\bar{v}, V	Average velocity
U	Velocity Fourier transform
TDL	Tunable Diode Laser
x	Longitudinal spatial dimension
α_i	m_{Air} power-law exponent
β_i	m_{Fuel} power-law exponent
γ_i	Pressure power-law exponent
Δx	Transducer axial spacing
π	3.14159...
ρ	Density
$\bar{\rho}$	Average density
ϕ	Equivalence ratio
ϕ'	Equivalence ratio perturbation
$\bar{\phi}$	Average equivalence ratio
\dagger	Matrix transpose

INTRODUCTION

Combustion instabilities in dry low-emissions combustors often result from a resonant interaction between unsteady heat release and acoustic modes of the system. These resonant oscillations tend to degrade combustor operability and can lead to flame blow-off, flashback, and large amplitude pressure fluctuations. Insight to predicting combustor stability

properties can be achieved by integrating a Flame Transfer Function (FTF) with an acoustic model to describe the flame-acoustic coupling of the system and the resulting unstable modes. The development of accurate FTF measurement and modeling techniques will be critical to the success of this prediction strategy. Modern gas turbine technology has been migrating towards lean premixed combustion in response to both increased environmental awareness and energy efficiency. Swirl stabilized combustion is a typical configuration where the swirl combined with distributed fuel injection is used to maximize mixing. However, complex interaction between the combustion and the acoustic and hydrodynamic flow field in a lean combustor makes for a difficult scenario to model. Furthermore, it is well established that lean premixed combustors are susceptible to thermoacoustic instabilities (1). The presence of instabilities result in increased noise, reduced engine performance, and a (possibly rapid) reduction in engine lifetime due to structural damage (2,3).

The acoustic instabilities as described by Rayleigh's Criterion (4) result from the unsteady interaction of heat release in the flame with pressure field's induced velocity. The sound intensity emitted by this thermal-acoustic interaction depends on the impedance along the boundaries and on a transfer function defining the response of the flame to velocity disturbances induced by the pressure field. As long as the power input due to the flame interaction exceeds the rate at which energy is dissipated at the boundaries then there is a growth of the internal pressure field and an increase in the acoustic levels. Naturally, a Flame Transfer Function (FTF) where the magnitude and phase of the heat release perturbation normalized by an input perturbation is a critical input to any acoustic model of a combustion system. Two typical input perturbations are a velocity perturbation imposed at a flame base or an equivalence ratio perturbation imposed on the fuel delivery system.

In addition to using the FTF as an input to an acoustic model, a measured FTF can be used as a coarse validation tool for CFD modeling of complex combustion systems. Many aspects of a CFD model must be correct (or nearly so) to reproduce a measured FTF and the unsteady accuracy of any model is exercised by comparing a computed FTF to a numerically calculated one over an extended frequency range. A further challenge is imposed when recognizing that periodically-excited unsteady systems can be unsteady in their response. In other words, the observed magnitude and phase of the global FTF are not steady values even for a steady input. This paper aims to introduce data analysis techniques that extract the unsteady behavior that is often missed when Fourier techniques are used in isolation.

EXPERIMENTAL SETUP

The major components of the swirl-stabilized, natural gas fueled combustor are shown in Figure 1. Compressed air is metered and then heated via a 900 kW electric heater. The main-air control valve tailors the overall flow rate. A siren

modulates a portion of the air while another control valve governs the air that bypasses the siren. For premixed conditions, fuel is introduced just down stream of the main control valve, and for partially-premixed conditions it is introduced into the swirling vanes of the fuel nozzle. The fuel used was natural gas (95.7 Mol% CH₄ with 1.6 Mole% C₂H₆, 1.9Mol% N₂, and 0.7 Mol% CO₂ + minor species). The fuel nozzle was located between the air plenum and a cylindrical quartz combustor terminated by a converging section to inhibit recirculation of laboratory air. The fuel nozzle possesses an annular region that was instrumented with a pair of phase matched piezoresistive pressure transducers. Additionally, the fuel nozzle was configured with a pair of angled sapphire windows that passed a tunable diode laser beam to measure the path-averaged methane concentration along a chord of the annulus (5). Chemiluminescence was collected from the test section using a fiber optic and a negative focal length lens to acquire light across the whole test section. The light from the fiber optic was collimated and spectrally separated into OH, CO₂ and CH channels using angle-tuned dichroic mirrors and narrow band-pass filters centered on 309 nm (OH), 360 nm (CO₂), and 430 nm (CH). The spectrally separated beams were then focused on UV sensitive Photomultiplier Tubes (PMT).

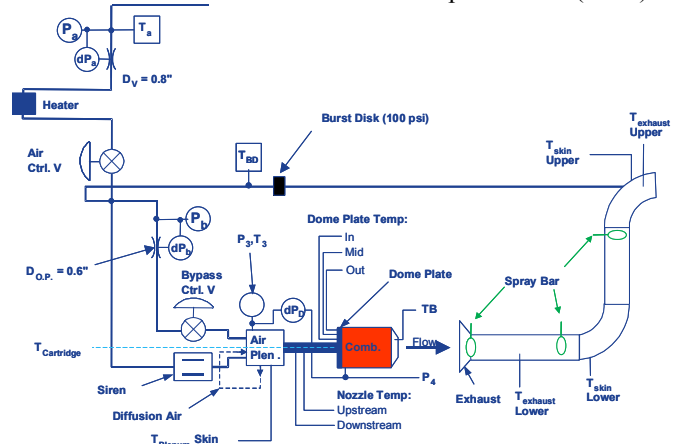


Figure 1. Schematic of the test rig.

EXPERIMENTAL TECHNIQUE

The dynamic response of a flame to a velocity perturbation can be captured by the following expression:

$$FTF(f) = \frac{q'/\bar{q}}{v'/\bar{v}}, \tag{1}$$

where the fluctuating quantities are normalized by their mean values. Heat release measurements, as inferred from chemiluminescence measurements, were acquired in a global (integrated across the combustor) fashion. It is understood that the use of chemiluminescence intensities as a marker for heat release rate is still a topic of investigation (6-11) a technique popularized by Schuermans (12-16) was used as it lends itself to quantitative evaluation of normalized heat release, indication

of the underlying physical mechanism (e.g., equivalence ratio fluctuations, or mass flow fluctuations) and by inference an extrapolation to partially premixed flames where equivalence ratio fluctuations will play a role. The technique is derived from essentially steady-state relationships between heat release and chemiluminescence. However, unsteady models strongly suggest these techniques perform well quantitatively (17). Velocity perturbations were measured using a Two-Microphone Method (TMM), a technique that lends itself well to the annular geometry of the swirl-stabilized burner with a center body.

Heat release perturbations

Schuermans' technique for a direct optical multi-signal method has been reviewed previously (18) and only the salient details from that review will be presented here.

The heat release rate (Q) can be given by the following energy-balance equation (assuming 100% combustion):

$$Q = m_{Air} \phi \cdot \left(\frac{m_{Fuel}}{m_{Air}} \right)_{stoich} \cdot H_{Fuel} \quad (2)$$

where m_{Fuel} and m_{Air} are the instantaneous values of the fuel and air mass flow rates respectfully, while H_{Fuel} is the fuel's chemical enthalpy, and ϕ is the equivalence ratio. A linearization of this equation yields:

$$\frac{Q'}{Q} = \frac{m'}{m} + \frac{\phi'}{\phi}, \text{ where } m \text{ is } m_{Air}. \quad (3)$$

To obtain the individual heat-release-rate contributions (m' and ϕ' fluctuations) consider the chemiluminescence intensity, I_i , of a relaxing chemical species (i). I_i has been shown to exhibit the following power law dependence on the air mass flow (m_{Air}) and the equivalence ratio ϕ :

$$I_i = k_i m_{Air}^{\alpha_i} \phi^{\beta_i} p^{\gamma_i} \quad (4)$$

where k_i , α_i , β_i , and γ_i are constants for species i . Fixing $\alpha_i = 1$ (19) and neglecting the pressure dependence for low-Mach number conditions, the resulting chemiluminescence signal can be characterized by,

$$I_i = k_i m_{Air} \phi^{\beta_i}. \quad (5)$$

Computing the linearization of the intensity signal on perturbations of air and fuel the following relationship is obtained:

$$\frac{I_i'}{I_i} = \frac{m'}{m} + \beta_i \frac{\phi'}{\phi} \quad (6)$$

Then, writing relationship for intensity out for N species in matrix form yields the following:

$$\begin{bmatrix} \frac{I_1'}{I_1} \\ \frac{I_1'}{I_1} \\ \vdots \\ \frac{I_n'}{I_n} \\ \frac{I_n'}{I_n} \end{bmatrix} = C_N \begin{bmatrix} \frac{m'}{m} \\ \frac{\phi'}{\phi} \end{bmatrix}, \text{ with } C_N = \begin{bmatrix} 1 & \beta_1 \\ \vdots & \vdots \\ 1 & \beta_n \end{bmatrix} \quad (7)$$

A calibration of the optical system is obtained by acquiring intensity signals from each of the PMT channels over the

anticipated range of air mass flow rate and fuel equivalence ratio. Equation 5 was fitted to each of the measured surfaces for each of the acquired species. By inverting C_N , an over-determined-matrix relationship is obtained between the heat release terms in equation 7 and the species signal intensities:

$$\begin{bmatrix} \frac{m'}{m} \\ \frac{\phi'}{\phi} \end{bmatrix} = C_N^\dagger \begin{bmatrix} \frac{I_1'}{I_1} \\ \frac{I_1'}{I_1} \\ \vdots \\ \frac{I_N'}{I_N} \\ \frac{I_N'}{I_N} \end{bmatrix} \quad (8)$$

Time resolved measurements of the intensity fluctuations can then be transformed into normalized heat release fluctuations and used in the definition of a flame transfer function in equation 1.

Heat release error estimation

To evaluate the systematic error contribution to the measurement, a set of calibrations were made before and after the test series. Figure 2 illustrates two sets of calibrations for a single species. One surface is a rainbow while the second surface is a 4-tiered rainbow to indicate that the surfaces did not migrate a great deal over a week's time. A set of β_i coefficients were fitted to the combination of data points and a Monte Carlo technique was applied to a defined set of air-mass-flow fluctuations and equivalence-ratio fluctuations letting the distribution of β_i vary by $\pm\sigma_\beta$ over 1000 realizations.

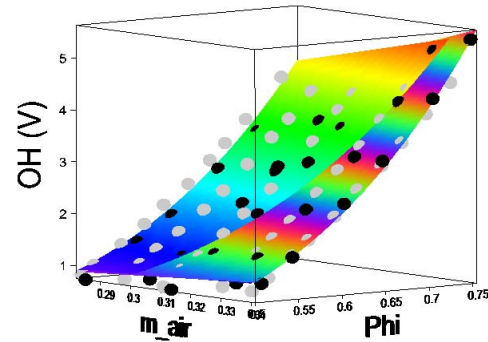


Figure 2. Example PMT signal over a range of air-mass flow rates and equivalence ratios.

The Monte Carlo technique was applied in 5 regions of the calibrations as indicated in Figure 3.

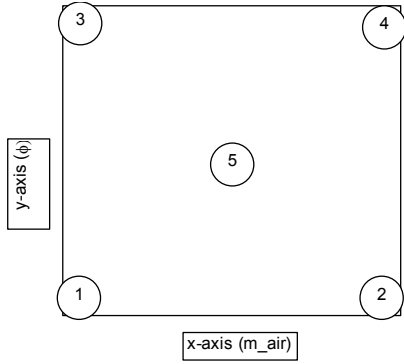


Figure 3. Calculation regions for Monte Carlo simulations.

Typical performance for the calibration set is shown for region 5 in Figure 3. In this figure, perturbations for fuel equivalence ratio and air mass-flow rates of 5 percent were used as inputs and the matrix inversion was executed over the range of distributed calibration coefficients. The result indicates the combined RMS error of the heat release measurements is good to +/- 8.2%.

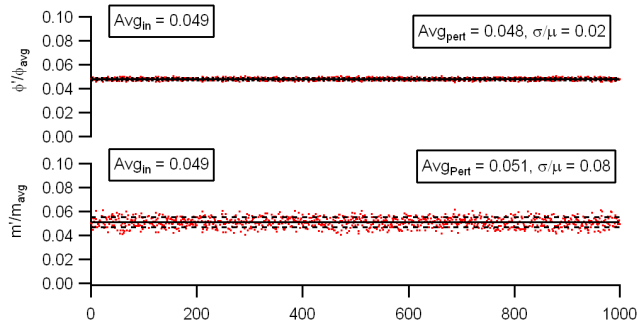


Figure 4 Monte Carlo error propagation estimate.

Velocity perturbations

To measure the velocity at the flame base, a Two-Microphone Method (TMM) is applied to the pressure distribution in the annular region of the burner tube. The adopted data analysis technique follows the direction taken by Waser and Crocker (20) where for inviscid one-dimensional flow with negligible momentum in the convective term, the momentum equation becomes,

$$\frac{\partial v}{\partial t} = -\frac{1}{\rho} \frac{\partial p}{\partial x} \quad (9)$$

By expressing the pressure gradient as a finite difference approximation, $(p_2 - p_1)/\Delta x$ and applying the Fourier Transform, equation 9 becomes,

$$U \cong \frac{j}{2\pi\Delta x} \frac{1}{\bar{\rho}} [P_2 - P_1] \quad (10)$$

Note, capital letters represent the Fourier transformed quantity.

Velocity error estimate

Two primary contributions to velocity error arise from uncertainties in the gain and mismatches in phase between the two transducers. To examine the potential instrumentation contribution to this error the pressure transducers were mounted in the closed endwall of a speaker-driven tube near the centerline. The length-to-diameter ratio was much greater than 30 letting one assume the pressure wave is planar near the endwall (opposite that of the speaker). Thus exposing the transducers to an identical pressure field.

Figure 5 illustrates the gain in signal between the two transducers. The inset accounts for the differences in static calibration. Two conclusions are that the static calibration is accurate over the frequency range of the experiment and second, that the worst-case gain error is 0.5 % which leads to a velocity error of less than 1%.

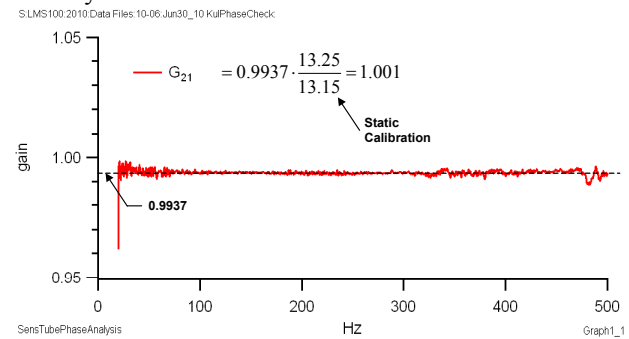


Figure 5. The measured gain relationship between two TMM pressure transducers.

Figure 6 illustrates the relative phase error between the two pressure transducers. Over the frequency range of interest the worst-case phase error is less than 0.25 degrees making the gain error the dominant error source.

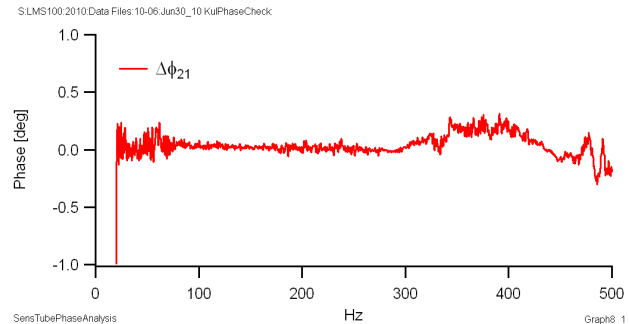


Figure 6. The phase relationship between two TMM pressure transducers.

Time resolved perturbation measurements

A common method to measure the magnitude and phase of a signal in a spectral bandwidth is to use Fourier Transform (FT) methods combined with Parseval's theorem (21) to compute the magnitude. The frequency band is usually defined by a feature's spectral width in the signal's power spectrum. Primary sources of "width" can be due to low-frequency

resolution in Fourier space (e.g., short temporal record lengths) where it is unlikely a specific frequency is resolved, phase deviations during the sample interval or unresolved sidebands caused by amplitude modulation of the signal. The latter two causes of spectral width are due to time-varying properties of the phenomenon and result in a "frequency modulated" signal. A different signal processing approach is required to elucidate the time-varying nature of non-stationary signals.

One method to unravel the frequency-modulated signals is to use lock-in-amplifier type techniques or Homodyne Detection (HD) (22). The following paragraphs outline the basics of the HD processing. This section ends with an example application of the technique to a self-excited combustion dynamics scenario to demonstrate the amplitude and phase capturing abilities of the technique.

A simplified schematic of the HD algorithm is shown in Figure 7 below. The sensor voltage signals are mixed non-linearly with a reference frequency equal to the band center of the spectral feature of interest with unity amplitude. In this work, the reference frequency is equal to the siren (or forcing) frequency. After mixing, the signal is low-pass filtered to recover the amplitude and phase information regarding the signal using common trigonometric identities. By using the same reference frequency on all the detector signals, a fixed phase reference is provided for all the detector signals.

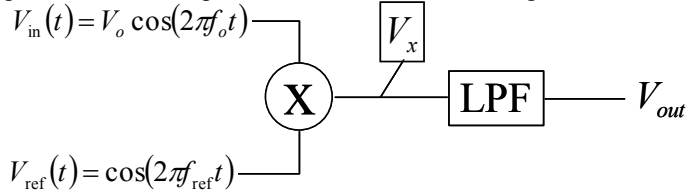


Figure 7. A schematic representation of homodyne detection.

An example graphical representation of the mixing process is shown in Figure 8. In the example, the signal amplitude is 3 volts at 205 Hz, and the reference signal at 200 Hz has unity amplitude. The result of the mixing in Fourier space is shown graphically in Figure 9 where the sum and difference frequencies are clearly illustrated. Additionally, the time-dependant mathematical description is an inset in the figure. Application of a low-pass filter to $V_x(t)$ removes the sum-frequency signal and permits recovery of the input-signal amplitude (after correcting by 1/2). Note, while the figures are shown in the Fourier domain, the output of the HD signal processing is a time-varying signal representative of the signal amplitude within the bandwidth of the low-pass filter. The bandwidth of the time-varying signal is equal to the low-pass filter cutoff. A good rule-of-thumb is to set the cutoff frequency to be at least as wide as the 1/e width of the amplitude spectra. Thereby capturing the unsteady behavior without capturing too much noise. This last point is analogous to the application of Parseval's theorem to FT signals. Meaning that the output is an

equivalent amplitude (but in the HD case the output is time-varying) of a periodic signal over the summed frequency span.

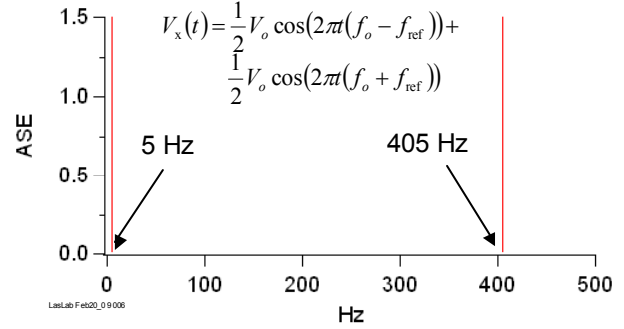


Figure 8. A graphical representation of mixing the signal with a reference frequency.

It is expected that the signal of interest will be out of phase with the reference signal. To capture the phase of the output signal it is best to illustrate it as a phasor as shown in Figure 9 where the input signal can be visualized as the vector sum of $V_x(t)$ and $V_y(t)$. The angle represents the phase offset (signal lag or lead) with respect to the reference signal

The process described above is parallelized into two threads where the reference signal for each thread is,

$$V_{ref}^x(t) = \cos(2\pi f_{ref} t), \quad (11)$$

$$V_{ref}^y(t) = \sin(2\pi f_{ref} t). \quad (12)$$

Note, everything is the same in the two threads except that the mixing is done with a pair of reference signals that are 90-deg. out of phase with each other. The amplitude and phase of the input signal are recovered using the following formulas:

$$V_o(t) = \sqrt{V_x^2 + V_y^2} \quad (13)$$

$$\phi(t) = \tan^{-1}\left(\frac{V_y}{V_x}\right) \quad (14)$$

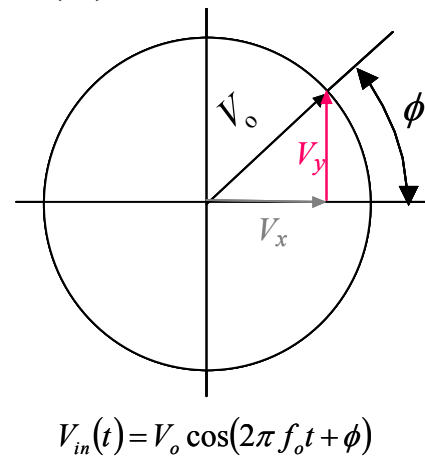


Figure 9, Phasor representation of the input signal.

RESULTS AND DISCUSSION

A set of results are reviewed for a nominal set of test conditions for a partially premixed case. The pressure drop (normalized to the ambient combustion pressure) was 2.6 percent. The average equivalence ratio for this case was 0.65. By design, industrial burners present a well-mixed fuel-air stream to the combustor base. To examine a burner's response to perturbations, the air is forced through a siren upstream of the combustor while the fuel injection stream is maintained constant. Thus, a combination of sources for heat release fluctuations exist; mass flow fluctuations and equivalence ratio fluctuations. The air pre-heat temperature was set to 300 °F (422 K), which permitted a comparison of velocity measurements using a high-temperature hotwire and longitudinal-mode velocity perturbations using the two microphone method. The siren frequency was adjusted between a nominal set of frequencies. Data is acquired at each step for 6 seconds. Velocity perturbations near the flame base were nominally 10% for this case.

Time resolved perturbation measurements

The first set of plots illustrate some time-varying measurements captured for a low-frequency portion of the frequency scan, 58 Hz. Figure 10 illustrates the time history of the collected emission centered near 309 nm (OH-channel) from a photomultiplier tube.

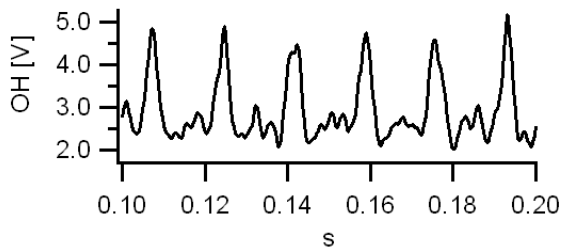


Figure 10. Time history of a PMT channel centered on OH emission.

Similar measurements are acquired for both a CO₂ channel and a CH channel. Using Schuermans' heat-release matrix calculation, the heat release contribution from equivalence ratio perturbations is calculated and compared with a measured equivalence ratio perturbation using a tunable diode laser. Figure 11 illustrates a sample time history of each of these measurements.

Figure 11 indicates that the heat-release perturbation based on the equivalence ratio qualitatively tracks the measured equivalence ratio. A slight phase delay is expected in the heat release measurement because the signals are acquired in the combustion section while the TDLAS measurement is acquired upstream of the combustor in a burner tube.

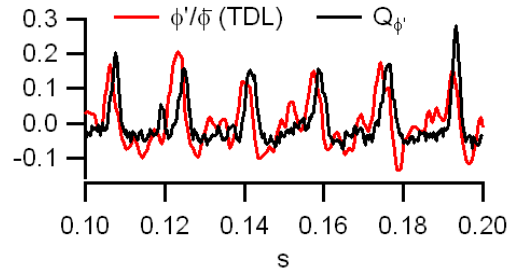


Figure 11. Equivalence-ratio-based heat-release measurements combined with direct equivalence ratio measurements using TDLAS.

The other quantity necessary for a flame transfer function measurement is a measurement of the velocity perturbation. Figure 12 illustrates a pair of measurements at a slightly higher frequency (90.3 Hz) that were acquired in the burner tube using both the TMM and a HW. Note, the average velocity in the burner tube was calculated using a mass balance and it was added to the TMM velocity measurement for comparison.

Agreement between the two measurement techniques is quite good. While the hotwire certainly indicates more high-frequency content, the two techniques present nearly equal coarse velocity fluctuations that are in phase. The purpose of the HW measurements was to validate the TMM technique for its accuracy in this non-ideal flow field. The TMM technique is used for the FTF measurements for two reasons. First, because it represents the acoustic velocity perturbation in a longitudinal mode while the single HW measurement will be sensitive to additional velocity components as well as small-scale turbulence. Second, the hot-wire technique has temperature limitations which hinders its application for realistic combustor inlet temperatures.

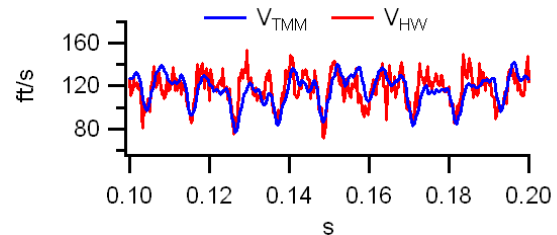


Figure 12. Velocity time history using a hotwire and TMM.

Homodyne detection measurements

The next series of plots demonstrate the variability of the gain and phase over the course of a 6-second, fixed-frequency measurement. In each of these plots measurands used to calculate the gain and phase of the transfer function were derived using homodyne detection. In Figure 13, three sets of measurements are presented for a forcing case at 106 Hz. In the top, left axis, the magnitude of the mass-fluctuation portion of the heat release is plotted versus time. In the top, right axis,

the magnitude of the normalized velocity perturbation is also plotted. The gain portion of the heat release due to mass fluctuations and the velocity perturbation FTF is illustrated in the bottom portion of the graph. The average gain at this condition is 1.2, but the variability indicated by the standard deviation is 0.17. However, there are short time intervals where the gain excursions nearly reach 2 (see 2.3 seconds and 4.4 seconds).

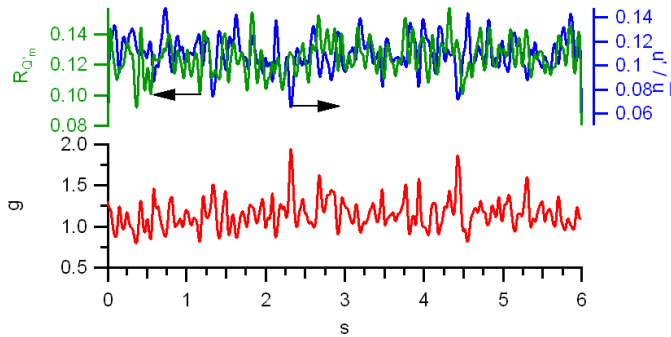


Figure 13. Gain calculation at a fixed frequency using measured Q' from mass flow perturbations and the velocity perturbations near the flame base.

Typically the distributions of gain tend to be normal with only a slight skewness due to the fact that theoretically very high gains could be supported while the minimum gain is only zero. To permit representation of any skewness, FTFs are presented using the median of the gain with upper and lower quartiles of the distribution plotted as error bars.

Phase time-history plots of heat-release parameters, velocity, and TDLAS equivalence ratio measurements are presented in Figure 14. Slowly varying (order of 1 second time constant) trends similar to this are found in all the phase measurements because the use of a fixed phase reference exposes gradual siren-frequency shifts. The frequency shift due to the siren in this case is less than 0.1 Hz (0.5 cycles over a 6-s interval). The HD technique is able to capture the variability in the relative phase measurements. The significance of these time-dependant calculations is they permit a measurement of the phase and its variability over a measurement interval

Flame transfer function measurements

Once the computed gain and phase relationships are acquired for each of the excitation frequencies at a test condition, the flame transfer function can be calculated. However, an additional intermediate step is to examine the perturbation amplitudes of each of the heat-release measurements along with the equivalence ratio perturbation measured with the TDLAS system. Figure 15 illustrates a comparison of these parameters where the (zero-to-peak) normalized perturbation amplitudes of the heat release quantities, and the TDLAS equivalence ratios are presented. For low-frequency excitation, the heat-release mechanism is dominated by the equivalence ratio fluctuations and the figure

illustrates this dependence drops off with increasing excitation frequency. Additionally, the same trend in equivalence ratio perturbations is captured by both the chemiluminescent technique and the TDLAS measurement. The bottom trace presents the measured phase using both FT techniques and HD techniques. Each method computes nearly the identical average phase. However, the HD technique also presents an indication of phase variability providing an opportunity for greater physical insight.

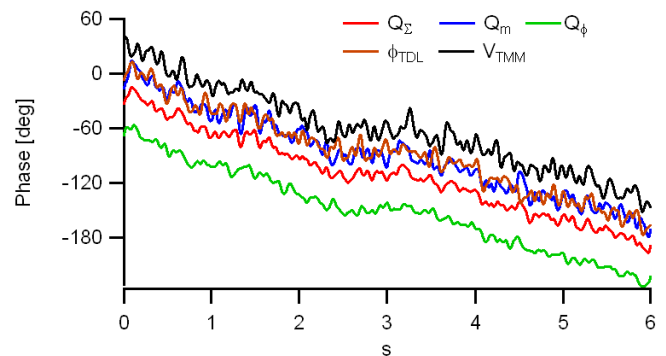


Figure 14. Phase time histories of Q' (sum), Q' (mass flow), Q' (equivalence ratio), TDLAS based equivalence ratio and TMM velocity.

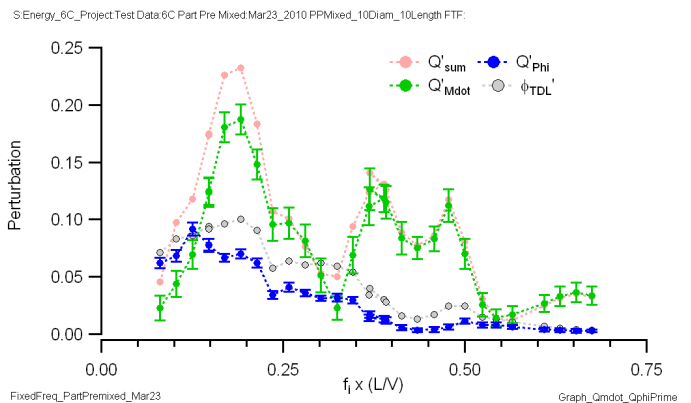


Figure 15. A representation of the measured perturbation magnitude of heat release and TDLAS-based equivalence ratio perturbations.

In a partially premixed condition, two FTF functions are available, the heat-release FTF using Q' from equivalence-ratio fluctuations and the measured equivalence ratio fluctuations. The second is the FTF using Q' from the mass-flow fluctuations and the velocity perturbations. These two FTFs are illustrated in Figure 16 and Figure 17 respectively. In each figure the top portion illustrates the coherence between the measured Q' and the perturbed quantity (e.g., equivalence ratio, or velocity). The middle curve depicts the calculated gain. The error bars indicate the upper and lower quartiles for the measurement variation over the 6-second interval. The bottom curve indicates phase difference measurements using both Fourier

transform methods and homodyne detection. The results from the Fourier transform method are depicted by red dots, and the open blue circles represent the phase difference determined using the HD technique. The blue error bars indicate the measured phase variance using the HD technique

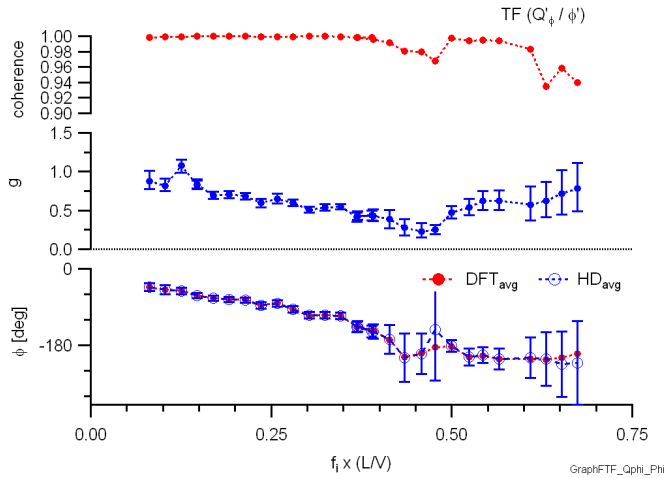


Figure 16. FTF between the heat release due to equivalence-ratio fluctuations and the measured equivalence ratio using TDLAS.

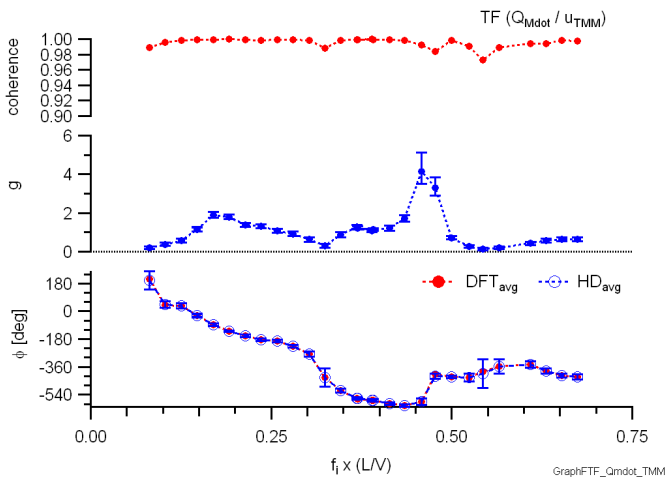


Figure 17. FTF between the heat release due to mass-flow fluctuations and the measured velocity perturbation using TMM.

The relative phase in both measurements indicate a nearly constant time delay, however in the mass-flow FTF there is an expected 180-deg phase shift that would be expected near a resonance condition. Note, the amplitude of the imposed perturbations (pressure, chemiluminescence, and velocity) was much stronger than the respective background signals present at quiescent conditions (i.e., no siren excitation). The larger variations in gain for the equivalence-ratio driven FTF are commensurate with a slight reduction in coherence. However, the driving mechanism for the increased variation is due to a reduction in both the equivalence-ratio based heat-release

perturbation level and a reduction in the measured equivalence ratio fluctuation using the TDL method.

CONCLUSIONS

Two pairs of nearly redundant measurements were shown to exhibit qualitatively very similar behavior. First, velocity measurements were performed using both a hot wire and a two-microphone method. The hotwire technique was used to validate that the accuracy of the TMM in a non-ideal swirling flow. Second, both the TDLAS measurement of equivalence-ratio fluctuations and the chemiluminescent measurement of heat release measurements due to equivalence ratio fluctuations yielded similar behavior. The combination of the two measurements permitted the measurement of a FTF that is dependant on equivalence ratio perturbations.

It is seen that Fourier transform techniques yield the same amplitude and phase as the median results derived from the homodyne detection technique. Use of the homodyne detection technique extracts a measurand's fluctuation in amplitude and phase. This feature will serve to help comparisons to numerically calculated FTFs in two ways. First, the measured fluctuations serve to provide an envelope for CFD models to target. Second, the multiple excursions of the gain or phase indicate that there are temporary conditions that exist in the combustor to support such high gains or migrations in phase. Time-accurate CFD results should statistically exhibit similar behavior if they faithfully capture the salient unsteady fluid-mechanic, acoustic, and kinetic phenomena that exist in the experimental combustor. Furthermore, the variations in gain and phase suggest a stochastic approach may be considered for FTF integration in combustion acoustic models.

REFERENCES

1. Putnam, A.A., "Combustion-Driven Oscillations in Industry," American Elsevier, NY, 1971.
2. Mongia, H.C., Held, T.J., Hsiao, G.C., and Pandalai, R.P. "Challenges and Progress in Controlling dynamics in Gas Turbine Combustors," *Journal of Propulsion and Power*, **19**,(5), 2003.
3. Lieuwen, T. and McManus, K., "Introduction: Combustion Dynamics in Lean-Premixed Prevapourised (LPP) Gas Turbines," *Journal of Propulsion and Power*, **19**,(5), 2003.
4. Rayleigh, J. W. S., "The Theory of Sound" Vol. II, Dover Publications, New York, 1945.
5. Li, H., Wehe, S.D., and McManus, K.R., "Real-time Equivalence Ratio Measurements in Gas Turbine Combustors with a Near-Infrared Diode Laser Sensor," 45th JPC, Denver, CO, August 2009.
6. Najm, H.N., Paul, P.H., Mueller, C.J., and Wyckoff, P.S., "On the Adequacy of Certain Experimental Observables as Measurements of Flame Burning Rate," *Combustion and Flame*, **113**, pp 312-332, 1998.

7. Meier, W., Weigand, P., Duan, X.R., and Giezendanner-Thoben, R., "Detailed Characterization of the Dynamics of Thermoacoustic Pulsations in a Lean Premixed Swirl Flame," *Combustion and Flame*, **150**, pp 2-26, 2007.
8. Nori, V., Seitzman, J., "Evaluation of chemiluminescence as a Combustion Diagnostic under Varying Operating Conditions," 46th AIAA Aerospace Sciences Meeting and Exhibit, Reno, Nevada, 2008.
9. Panoutsos, C.S., Hardalupas, Y., and Taylor, A.M.K.P., "Numerical Evaluation of Evaluation of Equivalence Ratio Measurement Using OH* and CH* chemiluminescence in premixed and Non-Premixed Methane-Air Flames," *Combustion and Flame*, **156**, pp. 273-291, 2009.
10. Hardalupas, Y., and Orain, M., "Local Measurements of the time-Dependent Heat Release Rate and Equivalence Ratio Using Chemiluminescent Emission from a Flame," *Combustion and Flame*, **139**, pp 188-207, 2004.
11. Samaniego, J.M., Egolfopoulos, F.N., and Bowman, C.T., "CO₂* Chemiluminescence in Premixed Flames," *combust. Sci. and Tech.*, **109**, pp183-203, 1995.
12. Paschereit, C., Schuermans, B., Polifke, W., and Mattson, O., A., "Measurement of Transfer matrices and Source terms of Premixed Flames," ASME 99-GT0133., Proc. ASME Turbo Expo 1999, Indianapolis, June 7-10, 1999.
13. Schuermans, B., "Modeling and Control of Thermoacoustic Instabilities," Ph.D. Thesis nr. 2800 EPFL Lausanne, Switzerland, 2003.
14. Schuermans, B., Polifke, W., and Paschereit, C., "Modeling Transfer Matrices of Premixed Flames and Comparison with Experimental Results," ASME 1999-GT-0132, Indianapolis, USA, June 7-10, 1999.
15. Schuermans, B., Guethe, F., and Mohr, W., "Optical transfer Function Measurements for Technically Premixed Flames," Proceedings of the ASME Turbo Expo 2008, GT2008-51500, Berlin, Germany, 2008.
16. Schuermans, B. Guethe, F., Pennel, D., Guyot, D., Paschereit, C.O., "Thermoacoustic Modeling of a Gas Turbine Using Transfer Functions Measured at Full Engine Pressure," Proceedings of the ASME Turbo Expo, 2009, GT2008-59605, Orlando, USA, 2009.
17. Shreekrishna and Lieuwen, T., "Flame Response to Equivalence ratio Fluctuations - Relationship Between Chemiluminescence and Heat Release," 45th Joint Propulsion Conference and Exhibit, Denver, CO, 2009.
18. Guyot, D. and Paschereit, "Optical Transfer Function Measurements for a Swirl Burner at Atmospheric Pressure," 45th JPC, AIAA 2009-5413, Denver CO, 2009.
19. Higgins, B., McQuay, M., Lacas, F., Rolon, J., Darabiha, N., and Candel, S., "Systematic Measurements of OH Chemiluminescence for Fuel-lean High-pressure, Premixed, Laminar Flames," *Fuel*, **80**, pp 1583-1591, 2001.
20. Waser, M.P., and Crocker M.J., "Introduction to the Two-Microphone Cross-Spectral method of Determining Sound Intensity," *Noise Control Engineering Journal*, **22**, No. 3, pp 76-85, 1984.
21. Smith, J.O., "Mathematics of the Discrete Fourier Transform (DFT)," W3K Publishing, May 2008.
22. Scofield, J.H. "A Frequency-Domain Description of a Lock-in Amplifier," *American journal of Physics*, **62**, (2), pp 129-133, 1994.